

TexDreamer: Towards Zero-Shot High-Fidelity 3D Human Texture Generation

Yufei Liu^{1†‡}, Junwei Zhu^{2‡}, Junshu Tang³, Shijie Zhang⁴, Jiangning Zhang²,
Weijian Cao², Chengjie Wang², Yunsheng Wu², Dongjin Huang^{1§}

¹ Shanghai University, Shanghai, China

² Tencent Youtu Laboratory

³ Shanghai Jiao Tong University, Shanghai, China

⁴ Fudan University, Shanghai, China

<https://ggxxii.github.io/texdreamer/>

Abstract. Texturing 3D humans with semantic UV maps remains a challenge due to the difficulty of acquiring reasonably unfolded UV. Despite recent text-to-3D advancements in supervising multi-view renderings using large text-to-image (T2I) models, issues persist with generation speed, text consistency, and texture quality, resulting in data scarcity among existing datasets. We present **TexDreamer**, the first zero-shot multimodal high-fidelity 3D human texture generation model. Utilizing an efficient texture adaptation finetuning strategy, we adapt large T2I model to a semantic UV structure while preserving its original generalization capability. Leveraging a novel feature translator module, the trained model is capable of generating high-fidelity 3D human textures from either text or image within seconds. Furthermore, we introduce **ArTicuLated humAn textureS** (ATLAS), the largest high-resolution ($1,024 \times 1,024$) 3D human texture dataset which contains 50k high-fidelity textures with text descriptions.

Keywords: human texture · multimodal · texture synthesis

1 Introduction

3D human texture plays a crucial and essential role in creating appealing 3D human models. UV map allows for seamless and accurate texturing of the 3D model by minimizing distortions, overlapping, and stretching. UV has gained widespread usage in various industrial fields, such as film production, gaming, and virtual reality. However, obtaining high-quality textures with reasonably unfolded UV can be a tedious and time-consuming task. In contemporary graphics production, the creation of 3D human textures mainly relies on pricey 3D scanners along with experienced texture painting artists. The scanning process

[†] Work is done during the internship at Tencent YouTu Lab.

[‡] Co-first author.

[§] Corresponding author.

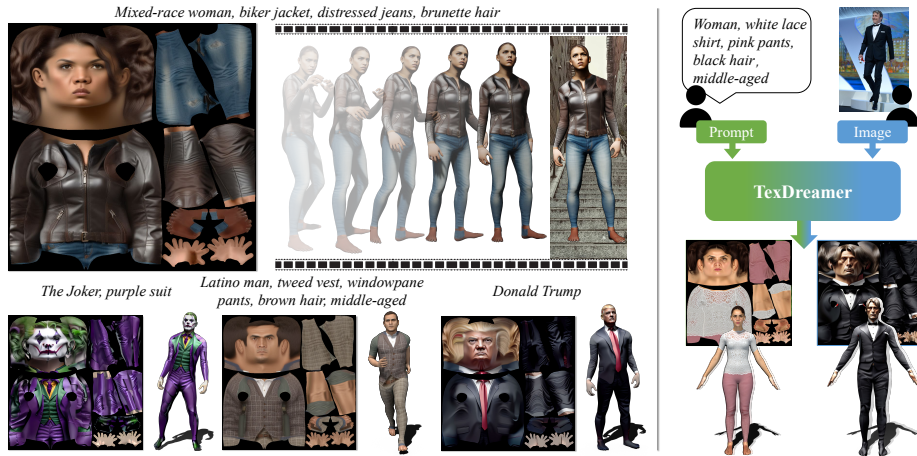


Fig. 1: Left: Overview of the ATLAS dataset. ATLAS is so far the largest high-resolution ($1,024 \times 1,024$) 3D human texture dataset paired with textual descriptions, including both real and fictional identities. **Right: Basic structure of our TexDreamer.** The first zero-shot high-fidelity human texture generation method that supports both text and image inputs.

necessitates a capturing system built with multi-camera array and structured light. Texture painting demands the expertise of trained artists proficient in using DCC software, *e.g.*, Substance Painter, ZBrush, and Photoshop. A well-structured human UV map often requires several weeks of dedicated effort.

Recent significant achievements in text-to-image fields have made it possible to directly generate 3D human models from textual descriptions using 3D priors. However, Human-oriented optimization methods [5, 18, 24, 26, 29, 66, 69] are time-consuming and suffer from limited texture quality due to rendering resolution constraints. Moreover, using these methods in practice requires mesh extraction algorithms such as marching cubes [34], which exhibits challenges in preserving UV layout and mesh topology, making the modification process highly inconvenient. Non-optimization texture generation methods primarily concentrate on objects, approaches like TEXTure [46], Latent-Paint [38], and Text2Tex [9] focus on completing the multi-view texture of given geometry using the Latent Diffusion Model (LDM) [47]. However, inconsistencies and gaps may occur when dealing with complex input models.

Apart from text, 2D images can also serve as a medium to texture 3D humans. Predicting texture from a single image mainly faces two challenges. For the visible parts, the UV mapping is influenced by the accuracy of pixel-to-surface correspondence estimation. For the invisible parts, the UV results rely on inpainting ability of the model. Without efficient high-quality data, this may lead to artifacts. Video datasets provide multi-view information, which aids in estimating the texture of the invisible parts. However, this approach requires a higher level of precision in pixel-to-surface correspondence estimation across frames. Additionally, video datasets are often limited in quantity.

To address these issues, we introduce TexDreamer, the first zero-shot multimodal high-fidelity human texture generation method that bridges the gap for 3D human texture creation. Our method can handle two of the most readily available raw data, text and image. This versatility makes our method more flexible and adaptable to different use cases. We first conduct an efficient texture adaptation finetuning for our Text-to-UV (T2UV). Training with high-quality sample textures acquired by a novel two-stage texture projection process, T2UV can attend to semantic and positional information of the specific UV structure while preserving the generalization capability of the original T2I model. For our Image-to-UV (I2UV), instead of predicting invisible parts of partial texture extracted by DensePose [16], we aim to connect image and UV in a more semantic latent space. We build a feature translator to translate the visual features extracted from the image to the textual feature space of T2UV. Trained with 4.2 million both real and synthetic human images, I2UV shows the highest texture quality and text consistency. Furthermore, we propose ATLAS (ArTicuLated humAn textureS) dataset, the largest high-resolution ($1,024 \times 1,024$) 3D human texture dataset. ATLAS contains 50k high-fidelity human textures conforming to the SMPL UV space. Each texture is paired with a detailed text description. See some examples in Fig. 1, our ALTAS dataset is distinguished by its high-fidelity and diverse character identities.

Our contributions can be summarized as follows:

- We introduce TexDreamer, the first zero-shot multimodal high-fidelity 3D human texture generation method accomplished through our efficient texture adaptation finetuning strategy and feature translator module design.
- We propose ATLAS, the largest high-resolution 3D human texture dataset, filling the vacancy in high-fidelity 3D human texture.
- Extensive experiments demonstrate that our method surpasses existing approaches regarding text consistency and UV quality for both modalities.

2 Related Work

Human-Related Datasets. Comparison of our ATLAS with existing human-related datasets is shown in Tab. 1. 3D scans have the highest precision but are the most difficult and time-consuming to acquire. [70] uses a custom-built multi-camera active stereo system to capture full-body human scans. [78] build THuman with dense DLSR rig, its subsequent [68] provides 500 scans with higher resolution. To predict clothing separately, there are also garment datasets [3, 35, 51, 65]. However, scan data usually has many vertices (often millions) and unstructured grids. Without additional processes, it’s hard to obtain texture maps from scans. In order to be free from complex hardware and high prices, a series of studies [1, 3, 12, 23, 31] have proven that neural networks can directly reconstruct 3D human from monocular RGB videos with 3D priors, *e.g.* the parametric human body model SMPL [33]. Human video datasets [1, 23, 31] generally appear as real human A-pose rotating videos. These kinds of data normally do not include any 3D information. While some work directly animates 2D image [61, 71],

Table 1: Comparisons of our ATLAS with existing human datasets. * indicates potential acquirable UV textures from 3D scans, and since texture acquirement depends on the setting, their UV resolution remains N/A.

Dataset	3D Shape	UV Textures	Texture Resolution	Text Description
BUFF [70]	✓	12*	N/A	✗
CAPE [35]	✓	15*	N/A	✗
X-Human [50]	✓	20*	N/A	✗
THuman [78]	✓	200*	N/A	✗
THuman2.0 [68]	✓	526*	N/A	✗
Digital Wardrobe [3]	✓	256*	N/A	✗
iPER [31]	✗	✗	N/A	✗
People-Snapshot [1]	✓	24	1,000×1,000	✗
SelfRecon [23]	✗	✗	N/A	✗
SMPLitex [6]	✗	100	512×512	✓
SURREAL [56]	✓	921	512×512	✗
ATLAS (Ours)	✓	50k	1,024×1,024	✓

to enhance asset usability and efficiency, many works focus on reconstructing 3D human from a single image [20, 49, 53, 60, 77] leveraging datasets [25, 32, 76]. Caused by acquisition difficulty, only a few datasets [1, 6, 27, 56] include UV textures. Registering scans, SURREAL [56] provides 921 UV textures. However, on account of the privacy policy, SURREAL UV textures all have the same average face. Lazova *et al.* [27] acquire scans using equipment from [54, 55] and purchases from commercial datasets [2, 45] to contribute a texture dataset, which is laborious and expensive. Closer to our texture generation method is SMPLitex [6], they use 10 UV textures from [1, 27] to fine-tune Stable Diffusion model [47], providing 100 UV textures with textual description. However, it lacks variation in identities and clothing. To the best of our knowledge, none of the existing human datasets has the same high-quality textures and rich information as ours.

Texture Generation from Text. Significant advancements in text-to-image have drawn considerable attention in the field of text-to-3D generation [10, 22, 30, 40, 43]. Human-oriented optimization methods [5, 18, 24, 26, 29, 69] with SMPL prior show great potential for generating 3D avatars with text. AvatarCLIP [18] refines the mesh appearance using [58] with CLIP score [44] supervising on rendering image. Leveraging Score Distillation Score (SDS) loss from DreamFusion [43], AvatarCraft [24] uses NeuS [58] combined with Instant-NGP [41] to optimize in canonical space. Zero-shot inference methods [9, 10, 38, 39, 46] show great advances in texturing 3D objects. Using PBR material [37], Fantasia3D [10] achieves realistic appearance modeling. Latent-NeRF [38] deploys SDS loss in the latent space of LDM [47]. TEXTure [46] and Text2Tex [9] update the multiple viewpoints and inpaint on the 3D mesh texture. Using only 10 training data, SMPLitex [6] lacks generalized ability and may produce faulty textures.

Texture Generation from Image. A group of work [6, 7, 15, 63, 74] dedicates to direct texture generation. Image-to-image generation approach [7, 8, 21] usually employs a GAN-based network to generate UV. Texformer [63] uses a

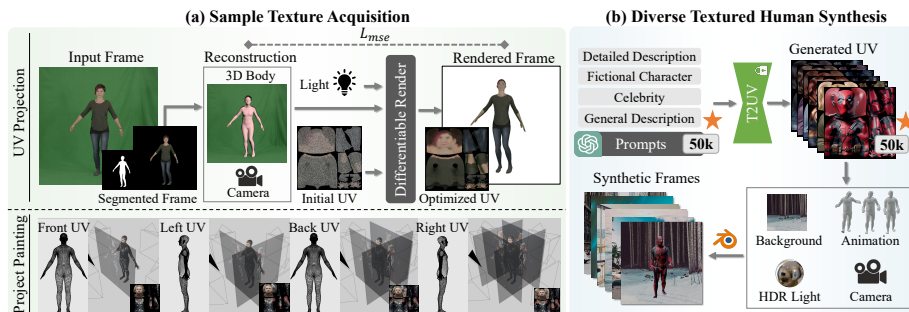


Fig. 2: Pipeline for generating synthetic data. Left: Sample texture acquisition. We first use a differentiable render to optimize UV from multi-view images, then further refine them by projection painting. Acquired sample textures with prompts are used to train T2UV in TexDreamer. Right: Diverse textured human synthesis. With the help of ChatGPT, we utilize T2UV to generate 50k human textures. Human images are rendered with animation sequence, background image, HDR lighting, and perspective camera. Orange stars indicate included data in our ATLAS dataset.

transformer-based network to align 2D human body segmentation with SMPL UV texture. Zhao *et al.* [74] adds part-based segmentation and enforces cross-view consistency. Stylepeople [15] introduces decoupled latent space of GAN to reconstruct hidden parts, but due to the imperfect generation model, it often produces unreasonable results. Based on diffusion models, SMPLitex [6] uses partial segmentation of Densepose as a condition to guide the stable diffusion model. Another line of work [27, 52] considers this task as an inpainting problem. Based on DensePose partial segmentation and texture, [27] uses a GAN-based network to complete texture map and displacement map. DINAR [52] uses StyleGAN2 to convert the input image into a neural texture. Not like existing methods that rely on 2D image segmentation, we build a feature translator to align human image and UV texture features in latent space.

3 ATLAS Dataset

Producing large-scale human textures with reasonably unfolded UV is inherently challenging due to the difficulty of acquiring such data for training. This section presents our ArTicuLated humAn textureS (ATLAS) dataset and describes its data generation strategy for TexDreamer training, including sample textures acquisition Sec. 3.1 and diverse textured human synthesis Sec. 3.2. See ATLAS visual pipeline in Fig. 2.

3.1 Sample Texture Acquisition

Obtaining well-structured human UV textures traditionally needs to register from scan data or paint by artists. We surpass both and propose first use UV Projection to optimize coarse human UV from multi-view images and then refine them with project painting. See the left of Fig. 2 for their visual process.

The core idea of UV projection is to minimize the difference between ground-truth frames and rendered frames. After segmentation, We exploit CLIFF [28] to estimate global rotation, joint pose, and 3D shape, along with camera parameters from masked frames. The initial UV map can be optimized through differentiable rendering. However, deviations exist between the estimated pose and the actual pose. We further conduct Project Painting to improve UV quality, which is a texture painting technique commonly used in CGI production. UV texture quality can be improved by alternating and modifying different SMPL UV maps from multiple view angles. The obtained UV data is used to train TexDreamer T2UV, see its detailed training method in Sec. 4.2.

To increase sample texture diversity and avoid T2UV overfitting, we use both real and generated multi-view images. For real human texture, we use videos from People-Snapshot [1] and iPER [31]. As for fictional characters, we rely on ControlNet [72] and DWpose [64] with pretrained LDM [47] to generate multi-view images of desired identities. Using eight SMPL A-pose for each character (rotation angle: 0, ± 45 , ± 90 , ± 135 , 180) and textual reinforcement, we manage to deal with the ID consistency problem of LDM. Specifically, we add corresponding orientation descriptions to constrain the generation, both positively and negatively. For instance, regarding the backside generation, we use “the back of, backside” as positive prompt, and the corresponding negative prompt is “face, front”.

3.2 Diverse Textured Human Synthesis

To synthesize diverse textured human images with identities for I2UV training, we composite T2UV-generated textures with animation, background, and HDR lighting. See the right of Fig. 2 for a visual pipeline.

Texture Generation. Generating a UV dataset using T2UV requires a large number of corresponding text descriptions. Expanding AvatarCLIP [18] classification, we depict our description as four categories: detailed description, fictional character, celebrity, and general description. Each has a designed structure. For detailed description, we first describe the appearance of a person with randomized descriptions for race or country, followed by gender, clothing, hairstyle, and age. For fictional characters and celebrities, we depict the person’s name and their common clothing. Celebrities add hairstyles to the structure of fictional characters. As for general description, each prompt contains one word or phrase to represent the category. See more prompt design in the supplementary. Leveraging ChatGPT [42], we generated a total of 50k prompts. We randomly select 20% of generation as ATLAS test set.

Composite Rendering. To enhance authenticity, we synthesize human images using Blender [4] with HDR image lighting and PBR human material shaders [37]. HDR lighting is developed by the Image Based Lighting (IBL) process [11], in which the light is sampled from a 360° panoramic image and reused to relight entire CG scene. IBL can simulate real scenes and ensure uniform lighting, we use HDR images as the “sunlight” to enrich lighting. For human material, we use bidirectional reflectance distribution function (BSDF), which

is a variant from Disney principled model also known as PBR shader [37]. See detailed settings in the supplementary.

Diversification of human postures is accomplished by AMASS [36], the largest human motion capture dataset, including more than 40 hours of motion data, spanning over 300 subjects. All the motion rate is set to 24, equal to the render frame rate, producing over 8.3 million rendering frames. Every motion sequence has a global transformation. To capture each human motion more completely, we set constraints on the rendering camera. Each perspective camera tracks the movement of “pelvis” joint and is located 5 meters in front of the mesh with 80mm focal length. The rendering sample for each pixel is set to 64.

Incorporating backgrounds contributes to a closer resemblance of real human images in the wild and increases the richness of synthetic images. Previous synthetic dataset SURREAL uses categories of kitchen, living room, bedroom, and dining room from LSUN [67]. LSUN image resolution is very low (256×256). To increase realism, we use royalty-free images from Pexels [13], including natural scenes, urban streets, indoor settings, abstract textures, and plain colors. Applying post-processing technique to compute input “alpha” channels and layer multiple rendering channels, we can combine the textured motion sequences with background images.

4 Zero-Shot Human Texture Generation

Generating large-scale realistic human textures with a uniform and semantic UV layout is inherently challenging due to the difficulty of acquiring efficient training data. We aim to use a small number of sample textures and leverage the generative and generalization capabilities of pretrained large-scale T2I models to establish a connection between common character generation and corresponding UV components. In this section, we provide a detailed description of TexDreamer, the first zero-shot multimodal high-fidelity 3D human texture generation method. We conduct a two-step training strategy, Text-to-UV (T2UV) Sec. 4.2 and Image-to-UV (I2UV) Sec. 4.3. We first train the T2UV module with efficient texture adaptation fine-tuning to allow texture generation from text. Then utilizing T2UV along with synthesized rendering images from ATLAS data generation, we train I2UV using a novel feature translator.

4.1 Preliminaries

Dreambooth [48] finetunes the entire parameters in LDM and creates a new checkpoint. Dreambooth can yield impressive results, but they come at a cost in terms of size. Textual Inversion [14], on the other hand, is faster because they learn to represent the provided concept through new “words” in the text embedding space. However, they only work for a single or a small handful of subjects. Different from the above two methods, low-rank adaption (LoRA) [19] method adds a new set of weights to the model, which can be used for general-purpose controlling. LoRA is initially proposed to fine-tune large language mod-

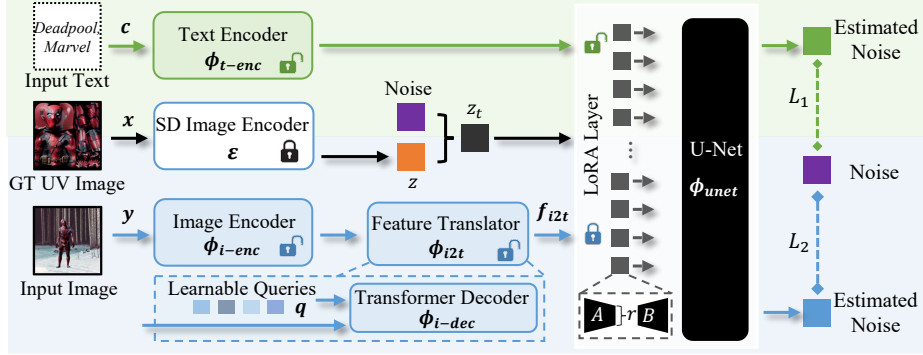


Fig. 3: Structure of TexDreamer. We conduct two training stages. For T2UV (green), we use LDM denoise loss \mathcal{L}_1 to optimize the text encoder and U-Net. For I2UV (blue), the feature translator ϕ_{i2t} map the input image feature encoded by ϕ_{i-enc} to a conditional feature f_{i2t} . We train I2UV by optimizing ϕ_{t-enc} and ϕ_{i-enc} with \mathcal{L}_2 .

els (LLMs), it learns weights by adding extra layers in the transformer cross-attention layer and uses low-rank matrices to learn the offset of parameters. This technique can also be applied in LDM.

4.2 Text-to-UV

For T2UV training, we conduct efficient texture adaptation fine-tuning. See the green flow of Fig. 3 for a visual training process of T2UV. Specifically, we add a few trainable parameters in each attention layer and train the model to learn the specific common concept of a small dataset through LoRA fine-tuning. Among all the finetune methods Sec. 4.1, LoRA strikes a good balance between training efficiency and the ability to fine-tune the model to generate specific concepts. Typically, the weight matrices in dense layers have full rank. LoRA shows that the updates to the weights also have a low “intrinsic rank” during adaptation. For the pre-trained weight matrix of LDM $W_{\phi_{unet}} \in \mathbb{R}^{d \times k}$, LoRA constrain the update by representing the latter with a low-rank decomposition, in this case $W_{\phi_{unet}} + \Delta W = W_{\phi_{unet}} + BA$, where $B \in \mathbb{R}^{d \times r}$, $A \in \mathbb{R}^{r \times k}$, and the rank $r \ll \min(d, k)$. During training, the trainable parameters are in A and B . For image-text input latent s , $\tilde{s} = W_{\phi_{tenc-unet}} s$, the modified forward pass yields:

$$\tilde{s} = W_{\phi_{tenc-unet}} s + \Delta W s = W_{\phi_{tenc-unet}} s + BAs. \quad (1)$$

LoRA uses a random Gaussian initialization for A and zero for B , then scales $W_{\phi_{tenc-unet}} s$ by $\frac{\alpha}{r}$, where α is a constant in r . The input GT UV image x is encoded with SD image encoder \mathcal{E} and the input text is encoded by ϕ_{t-enc} . Due to the large number of hyper-parameters of LDM, there is no fixed universal configuration during training. Using sample texture acquired from Sec. 3.1 together with their prompts c , we train T2UV via:

$$L_1 := \mathbb{E}_{\mathcal{E}(x), c, \epsilon \sim \mathcal{N}(0,1), t} \left[\|\epsilon - \phi_{unet}(z_t, t, \phi_{t-enc}(c))\|_2^2 \right], \quad (2)$$

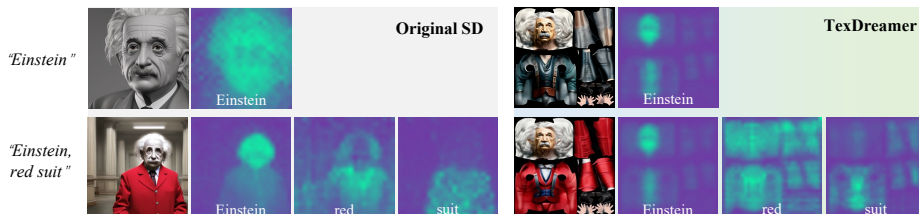


Fig. 4: Comparison of attention maps between the original SD and TexDreamer T2UV. The response area of the original SD is random, while T2UV consistently maps the prompts to the learned UV structure.

where both text encoder ϕ_{t-enc} and U-Net ϕ_{unet} are jointly optimized by Eq. (2).

With appropriate scale initialization, tuning α and r is nearly the same as tuning the learning rate, slight change may result in evident differences. In order to find the best α and r for optimizing ϕ_{t-enc} and ϕ_{unet} , other than \mathcal{L}_1 value, we mainly depend on quantitative measurement CLIP score [44]. For each setting, we calculate CLIP score on rendered T pose images and the corresponding prompts. To enhance the text-image consistency, we further employ an alignment enhancement strategy. After training with sample textures, we use the trained T2UV to generate 4 textures and only select 1 texture with the highest CLIP score for each prompt in ATLAS. The final T2UV we use for I2UV has the best text consistency, see Sec. 5.4 for T2UV ablation study. Moreover, the number of training samples can also influence model capabilities, see more experiments regarding this in the supplementary.

After extensive experiments, we find that T2UV inherits the generalization capabilities of the original SD model while adapting generation to a semantic UV layout. With the same text input, the attention response area of the original SD is random, while TexDreamer T2UV consistently maps the texts to the learned UV structure, see comparisons in Fig. 4. This learned structural information indicates that TexDreamer has the potential to generate a large-scale of human textures with various identities and clothing.

4.3 Image-to-UV

For predicting invisible textures from 2D human images, our key insight is that different structures of human images and UV textures can be connected with more semantic medium. In this case, we use the textual feature.

Training strategy of I2UV depends on synthetic textured human images from ATLAS and previously trained T2UV, see the blue flow in Fig. 3 for a visual process. Inspired by [75], we build a novel feature translator to transform input 2D image feature to the conditional text feature space of T2UV. We use image encoder ϕ_{i-enc} from CLIP [44] to extract visual features f_{voken} from rendered 2D image y . The feature translator translates visual features to textual features f_{i2t} , which includes a two-layer MLP model ϕ_{MLP} , a three-layer of transformer decoder ϕ_{i-dec} , and a learnable query sequence q . The translated feature $f_{i2t} \in$

$\mathbb{R}^{L \times \hat{d}}$ is then formulated as:

$$f_{i2t} := \phi_{i-dec}(\phi_{MLP}(f_{voken}), q) \in \mathbf{R}^{L \times \hat{d}}, \quad (3)$$

where L is the maximum input length of text encoder ϕ_{t-enc} and \hat{d} is the dimension of LDM encoder \mathcal{E} output feature. In our case, $f_{i2t} \in \mathbb{R}^{77 \times 1,024}$.

In order to constrain T2UV generation with the input image, the mapped feature f_{i2t} functions as a condition in the generation process. When training, the generated UV texture, as the ground truth, is first encoded into a latent feature z_0 through LDM image encoder. The noisy feature z_t is obtained by adding noise ϵ to z_0 . As f_{i2t} is essentially a text feature, similar to $\phi_{t-enc}(c)$, it can be directly used in training, we optimize the image encoder ϕ_{i-enc} and feature translator ϕ_{i2t} with LDM denoise loss:

$$\begin{aligned} f_{i2t} &:= \phi_{i2t}(\phi_{i-enc}(y)), \\ L_2 &:= \mathbb{E}_{\mathcal{E}(x), y, \epsilon \sim \mathcal{N}(0,1), t} \left[\|\epsilon - \phi_{unet}(z_t, t, f_{i2t})\|_2^2 \right]. \end{aligned} \quad (4)$$

5 Experiments

5.1 Experimental Setup

Implementation Details. For training T2UV, we use stable-diffusion-2-1 and clip-vit-large-patch14-336. The rank and α for ϕ_{unet} is 128, for ϕ_{t-enc} is 16. Each training uses batch size 8, with a total of 2,000 training steps. The optimizer is AdamW, with a learning rate set to 0.0001 and a constant scheduler with 100 warm-up steps. To improve training efficiency, we followed [17] and set the SNR- γ to 5. During inference, the weight of T2UV is set to 1.0, and we use the results of 32 steps. For training I2UV, based on T2UV, we use the same batch size but add training steps to 20,000, change the learning rate to $1e-5$, and set weight decay in regularization at 0.01. All training is conducted on a single Nvidia A100 GPU.

Evaluation Metrics. For T2UV, we use CLIP score [44] to measure consistency between generated textures and input texts. For all calculations, we render generated textures with SMPL neutral body in T-pose using Pytorch3D with the same perspective camera, lighting, and material. For I2UV, previous methods [57, 62, 63, 74] mainly use SSIM [59] and LPIPS [73] compute between the renderings and ground-truth images. However, affected by the accuracy of human pose estimation, these metrics can not fully measure the reconstructed texture quality. Since we have texture ground truth and corresponding text, we propose to use Mean Squared Error (MSE) and CLIP score to evaluate both texture quality and text consistency.

5.2 Qualitative Comparison

T2UV. We compare TexDreamer T2UV with state-of-the-art texture generation methods, including Text2Tex [9], TEXTure [46], Latent-Paint [38], Fantasia3D [10], and SMPLitex [6]. As shown in Fig. 5, our generation achieves the

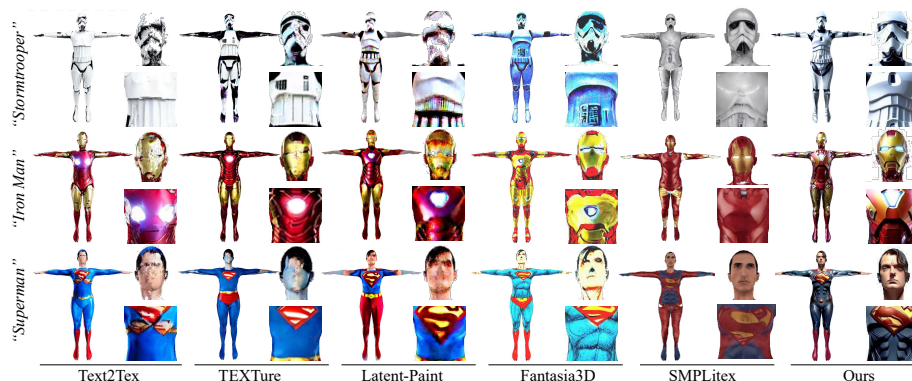


Fig. 5: Qualitative comparison of texture generation from text. We compare TexDreamer with state-of-the-art texture generation methods, including Text2Tex [9], TEXTure [46], Latent-Paint [38] and Fantasia3D [10]. Our results clearly achieve the finest facial details and the highest overall quality. Please zoom in for a better view.

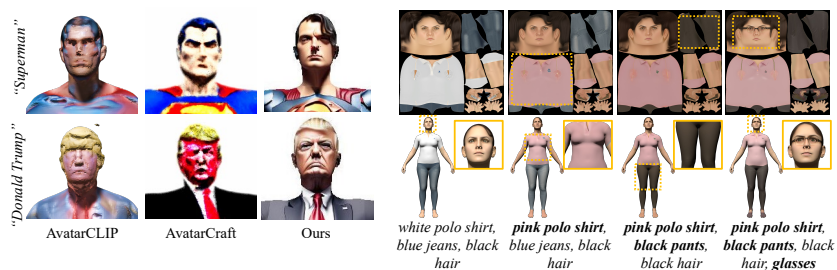


Fig. 6: Left: Qualitative comparison with AvatarCLIP [18] and AvatarCraft [24]. Our method has more realistic head avatars. Right: Texture editing. TexDreamer can use text to edit generated texture details, *e.g.*, clothing style, color, and accessories.

highest overall quality and the finest facial details. Since human-oriented optimization methods require a long time, see Tab. 2, we choose the first [18] and most current advanced [24] open source method to compare. They both have additional optimization steps in the facial area. We use identities in their showcase, left of Fig. 6 shows their results lack realism in texture colors and facial features. See more generation results of TexDreamer in the supplementary.

I2UV. We compare image-to-uv with the leading method Texformer [63] and SMPLitex [6]. We evaluate both on Texformer training dataset Market-1501 [76] and our ATLAS test set. See visual comparisons in Fig. 7. Our method achieves remarkably faithful identities and outstanding texture realism.

5.3 Quantitative Comparison

T2UV. The rendering of textured 3D human from text should closely resemble the input text at the reference view, and demonstrate consistent semantics with the reference under novel views. We evaluate these two aspects with CLIP

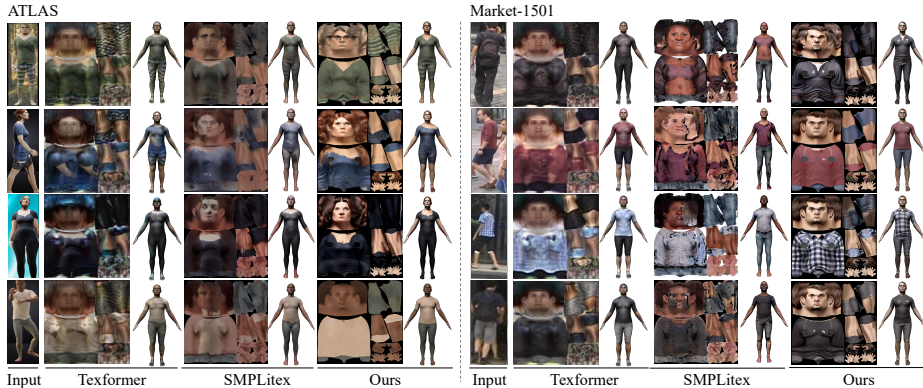


Fig. 7: Qualitative comparison with UV generation from image. We compare with advanced Texformer [63] and SMPLitex [6] on our ATLAS dataset (Left) and Market-1501 [76] (Right). Please zoom in to compare texture completeness and quality.

score [44], which computes the semantic similarity between the novel view and the reference. To evaluate T2UV text consistency more comprehensively, in addition to the basic rendering of SMPL in Sec. 5.1, we add three more views (azim = 0, 90, 180, 270). Due to the high consumption of time and resources, we only compare efficiency with AvatarCraft. As shown in Tab. 2, our method is the most efficient and achieves the best text consistency.

I2UV. With generated and collected textures as ground truth, we first use MSE to compare I2UV with advanced image-to-UV method Texformer [63] and Smplitex [6]. MSE computes the average of the squares between predicted and actual values. The smaller the MSE, the higher texture generation quality of the model. We randomly extract two frames from ATLAS test set as input. Furthermore, we evaluated text consistency of each texture using CLIP score with paired rendering and text description. Tab. 4 shows TexDreamer I2UV achieves the best result on both measurements.

Table 2: Quantitative comparison of generating human texture from text. “-T” means TexDreamer T2UV, we show compared inference methods (up) and optimization methods (middle) results. CLIP score of AvatarCraft is not reported due to the high consumption of time and resources.

Method	GPU (GiB)	Time (mins) ↓	CLIP Score ↑
Text2Tex [9]	20.31	~ 14.35	29.962
TEXTure [46]	12.05	~ 2.38	27.298
Latent-Paint [38]	11.46	~ 13.95	26.378
Fantasia3d [10]	12.42	~ 14.50	30.557
SMPLitex [6]	7.77	~ 0.31	22.998
AvatarCLIP [18]	37.74	~ 360	29.422
AvatarCraft* [24]	26.65	~ 480	-
Ours-T2UV	5.71	~ 0.17	31.297

Table 3: User study on texture generation from text. Our result has the highest image quality and test consistency.

Method	Text Consistency \uparrow	Image Quality \uparrow
Text2Tex [9]	1.919	1.641
TEXTure [46]	2.003	1.744
Latent-Paint [38]	1.878	1.456
Fantasia3D [10]	2.089	1.904
AvatarCLIP [18]	1.752	1.341
TexDreamer (Ours)	4.019	4.244

Table 4: Quantity comparison and ablation study of TexDreamer I2UV. “fixed ϕ_{i-enc} ” means we don’t train the image encoder in I2UV.

Method	MSE \downarrow	CLIP Score \uparrow
Texformer [63]	0.1148	21.811
SMPLitex [6]	0.0783	22.488
Ours-I2UV (fixed ϕ_{i-enc})	0.0632	26.138
Ours-I2UV (full)	0.0442	27.334

Table 5: Ablation study of TexDreamer T2UV. Our setting has the highest text consistency.

$\phi_{unet}r$	$\phi_{unet}\alpha$	$\phi_{t-enc}r$	$\phi_{t-enc}\alpha$	CLIP Score \uparrow
128	128	8	8	28.64
128	128	16	16	29.29
128	128	32	32	28.36
64	64	16	16	28.20
192	192	16	16	29.19

User Study. We further conduct a user study to evaluate texturing 3D humans using text. Tab. 3 indicates that our method has the highest preference and resembles closest to corresponding text. We use the same rendering view images, and invite 14 participants to rate on a scale of 1-5 about “the quality of overall texture” and “consistency with text description”. Each participant is randomly assigned with the same amount of comparisons.

5.4 Ablation Study

For training texture generation from text, we add a few trainable parameters in each attention layer, a slight change of rank and α in LoRA can greatly impact the generation result. We conducted ablation experiments on r and α of U-Net and text encoder. For ablation purposes, we reduce the training steps in Sec. 5.1 setting, others remain the same. Tab. 5 shows that our T2UV has the highest text consistency. For I2UV, we compare a fixed text encoder and full I2UV module on ATLAS test set, see Tab. 4. Our full model has the highest image similarity and text consistency.

6 Applications

Texture Editing. TexDreamer can use text to edit 3D human appearance generation, details to clothing style (both upper and lower garments), accessories, *etc.*, see Fig. 6. This allows fast and precise alterations of characters designed by artists, making our method more flexible and adaptable to concept character design in the film or game industry. The visual results also indicate that our

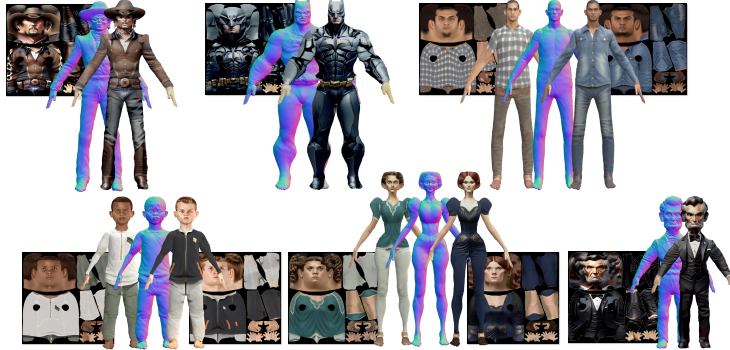


Fig. 8: Texturing dressed avatars. Our human textures can be applied to complex dressed meshes generated by text-to-3d method. We show some examples generated by TADA [29] with synthetic UV texture generated by TexDreamer.

method can generate human textures with different clothing while preserving the identity, which additionally opens doors for a fast virtual try-on.

Texturing Dressed Avatars. We further explored the application of our generated textures for more complex geometry. As shown in Fig. 8, our generated textures can integrate with complex human mesh and produce more authentic human-like characters. Specifically, we leverage the most advanced text-to-3D-avatar generation method TADA [29]. We apply the synthetic textures from TexDreamer by modifying the mesh initialization process, allowing it to density mesh while preserving the original UV information. This application shows that TexDreamer empowers users to create personalized characters with ease, which could be laborious for traditional 3D modeling techniques.

7 Conclusions

We propose the first zero-shot multimodal high-fidelity 3D human texture generation model, TexDreamer. Adapting large T2I model generative ability to unique UV structure with efficient texture adaptation fine-tuning and a novel feature translator, TexDreamer exhibits faithful identity and clothing for texturing 3D humans using texts or images. Enabling a more diverse range of human-like avatar generation. Furthermore, we construct ATLAS, the most extensive high-resolution ($1,024 \times 1,024$) 3D human texture dataset with a uniform and semantic UV layout, filling the absence of high-quality human UV data. Extensive experiments demonstrate that our method surpasses existing approaches in terms of text consistency and UV quality.

Limitations and Social Impacts. While TexDreamer shows promising results, it still has several limitations. I2UV is not based on Densepose segmentation, when applied to real-life cases, some output may not strictly align with the input clothing pattern. Producing realistic human texture, Texformer has the potential to influence virtual human industries. However, it also raises ethical and privacy concerns, as the technology could potentially be used for creating deepfakes.

References

1. Alldieck, T., Magnor, M., Xu, W., Theobalt, C., Pons-Moll, G.: Video based reconstruction of 3d people models. In: Proceedings of the IEEE Conference on Computer Vision and Pattern Recognition. pp. 8387–8397 (2018) [3](#), [4](#), [6](#)
2. XYZ: 4D Scanned People Character Animation Software. <https://secure.xyz-design.com/> (2023) [4](#)
3. Bhatnagar, B.L., Tiwari, G., Theobalt, C., Pons-Moll, G.: Multi-garment net: Learning to dress 3d people from images. In: Proceedings of the IEEE/CVF international conference on computer vision. pp. 5420–5430 (2019) [3](#), [4](#)
4. Blender - a 3D modelling and rendering package: <https://www.blender.org/> (2023) [6](#)
5. Cao, Y., Cao, Y.P., Han, K., Shan, Y., Wong, K.Y.K.: Dreamavatar: Text-and-shape guided 3d human avatar generation via diffusion models. arXiv preprint arXiv:2304.00916 (2023) [2](#), [4](#)
6. Casas, D., Trinidad, M.C.: Smlitex: A generative model and dataset for 3d human texture estimation from single image. arXiv preprint arXiv:2309.01855 (2023) [4](#), [5](#), [10](#), [11](#), [12](#), [13](#)
7. Cha, S., Seo, K., Ashtari, A., Noh, J.: Generating texture for 3d human avatar from a single image using sampling and refinement networks. In: Computer Graphics Forum. vol. 42, pp. 385–396. Wiley Online Library (2023) [4](#)
8. Chang, S., Cho, J., Oh, S.: Texture generation using dual-domain feature flow with multi-view hallucinations. In: Proceedings of the AAAI Conference on Artificial Intelligence. vol. 36, pp. 203–211 (2022) [4](#)
9. Chen, D.Z., Siddiqui, Y., Lee, H.Y., Tulyakov, S., Nießner, M.: Text2tex: Text-driven texture synthesis via diffusion models. arXiv preprint arXiv:2303.11396 (2023) [2](#), [4](#), [10](#), [11](#), [12](#), [13](#)
10. Chen, R., Chen, Y., Jiao, N., Jia, K.: Fantasia3d: Disentangling geometry and appearance for high-quality text-to-3d content creation. arXiv preprint arXiv:2303.13873 (2023) [4](#), [10](#), [11](#), [12](#), [13](#)
11. Debevec, P.: Rendering synthetic objects into real scenes: Bridging traditional and image-based graphics with global illumination and high dynamic range photography. In: Acm siggraph 2008 classes, pp. 1–10 (2008) [6](#)
12. Feng, Y., Yang, J., Pollefeys, M., Black, M.J., Bolkart, T.: Capturing and animation of body and clothing from monocular video. In: SIGGRAPH Asia 2022 Conference Papers. pp. 1–9 (2022) [3](#)
13. Free Stock Photos, Royalty Free Stock Images amd Copyright Free Pictures: Pexels, <https://www.pexels.com/> [7](#)
14. Gal, R., Alaluf, Y., Atzmon, Y., Patashnik, O., Bermano, A.H., Chechik, G., Cohen-Or, D.: An image is worth one word: Personalizing text-to-image generation using textual inversion. arXiv preprint arXiv:2208.01618 (2022) [7](#)
15. Grigorev, A., Isakov, K., Ianina, A., Bashirov, R., Zakharkin, I., Vakhitov, A., Lempitsky, V.: Stylepeople: A generative model of fullbody human avatars. In: Proceedings of the IEEE/CVF Conference on Computer Vision and Pattern Recognition. pp. 5151–5160 (2021) [4](#), [5](#)
16. Güler, R.A., Neverova, N., Kokkinos, I.: Densepose: Dense human pose estimation in the wild. In: Proceedings of the IEEE conference on computer vision and pattern recognition. pp. 7297–7306 (2018) [3](#)
17. Hang, T., Gu, S., Li, C., Bao, J., Chen, D., Hu, H., Geng, X., Guo, B.: Efficient diffusion training via min-snr weighting strategy. arXiv preprint arXiv:2303.09556 (2023) [10](#)

18. Hong, F., Zhang, M., Pan, L., Cai, Z., Yang, L., Liu, Z.: Avatarclip: Zero-shot text-driven generation and animation of 3d avatars. arXiv preprint arXiv:2205.08535 (2022) [2](#), [4](#), [6](#), [11](#), [12](#), [13](#)
19. Hu, E.J., Shen, Y., Wallis, P., Allen-Zhu, Z., Li, Y., Wang, S., Wang, L., Chen, W.: Lora: Low-rank adaptation of large language models. arXiv preprint arXiv:2106.09685 (2021) [7](#)
20. Huang, Y., Yi, H., Xiu, Y., Liao, T., Tang, J., Cai, D., Thies, J.: TeCH: Text-guided Reconstruction of Lifelike Clothed Humans. In: International Conference on 3D Vision (3DV) (2024) [4](#)
21. Isola, P., Zhu, J.Y., Zhou, T., Efros, A.A.: Image-to-image translation with conditional adversarial networks. In: Proceedings of the IEEE conference on computer vision and pattern recognition. pp. 1125–1134 (2017) [4](#)
22. Jain, A., Mildenhall, B., Barron, J.T., Abbeel, P., Poole, B.: Zero-shot text-guided object generation with dream fields. In: Proceedings of the IEEE/CVF Conference on Computer Vision and Pattern Recognition. pp. 867–876 (2022) [4](#)
23. Jiang, B., Hong, Y., Bao, H., Zhang, J.: Selfrecon: Self reconstruction your digital avatar from monocular video. In: Proceedings of the IEEE/CVF Conference on Computer Vision and Pattern Recognition. pp. 5605–5615 (2022) [3](#), [4](#)
24. Jiang, R., Wang, C., Zhang, J., Chai, M., He, M., Chen, D., Liao, J.: Avatarcraft: Transforming text into neural human avatars with parameterized shape and pose control. 2023 IEEE/CVF International Conference on Computer Vision (ICCV) pp. 14325–14336 (2023), <https://api.semanticscholar.org/CorpusID:257834153> [2](#), [4](#), [11](#), [12](#)
25. Jiang, Y., Yang, S., Qiu, H., Wu, W., Loy, C.C., Liu, Z.: Text2human: Text-driven controllable human image generation. ACM Transactions on Graphics (TOG) **41**(4), 1–11 (2022) [4](#)
26. Kolotouros, N., Alldieck, T., Zanfir, A., Bazavan, E.G., Fieraru, M., Sminchisescu, C.: Dreamhuman: Animatable 3d avatars from text. arXiv preprint arXiv:2306.09329 (2023) [2](#), [4](#)
27. Lazova, V., Insafutdinov, E., Pons-Moll, G.: 360-degree textures of people in clothing from a single image. In: 2019 International Conference on 3D Vision (3DV). pp. 643–653. IEEE (2019) [4](#), [5](#)
28. Li, Z., Liu, J., Zhang, Z., Xu, S., Yan, Y.: Cliff: Carrying location information in full frames into human pose and shape estimation. In: European Conference on Computer Vision. pp. 590–606. Springer (2022) [6](#)
29. Liao, T., Yi, H., Xiu, Y., Tang, J., Huang, Y., Thies, J., Black, M.J.: TADA! Text to Animatable Digital Avatars. In: International Conference on 3D Vision (3DV) (2024) [2](#), [4](#), [14](#)
30. Lin, C.H., Gao, J., Tang, L., Takikawa, T., Zeng, X., Huang, X., Kreis, K., Fidler, S., Liu, M.Y., Lin, T.Y.: Magic3d: High-resolution text-to-3d content creation. In: Proceedings of the IEEE/CVF Conference on Computer Vision and Pattern Recognition. pp. 300–309 (2023) [4](#)
31. Liu, W., Piao, Z., Min, J., Luo, W., Ma, L., Gao, S.: Liquid warping gan: A unified framework for human motion imitation, appearance transfer and novel view synthesis. In: Proceedings of the IEEE/CVF International Conference on Computer Vision. pp. 5904–5913 (2019) [3](#), [4](#), [6](#)
32. Liu, Z., Luo, P., Qiu, S., Wang, X., Tang, X.: Deepfashion: Powering robust clothes recognition and retrieval with rich annotations. In: Proceedings of the IEEE conference on computer vision and pattern recognition. pp. 1096–1104 (2016) [4](#)

33. Loper, M., Mahmood, N., Romero, J., Pons-Moll, G., Black, M.J.: Smpl: A skinned multi-person linear model. In: *Seminal Graphics Papers: Pushing the Boundaries, Volume 2*, pp. 851–866 (2023) [3](#)
34. Lorensen, W.E., Cline, H.E.: Marching cubes: A high resolution 3d surface construction algorithm. In: *Seminal graphics: pioneering efforts that shaped the field*, pp. 347–353 (1998) [2](#)
35. Ma, Q., Yang, J., Ranjan, A., Pujades, S., Pons-Moll, G., Tang, S., Black, M.J.: Learning to dress 3d people in generative clothing. In: *Proceedings of the IEEE/CVF Conference on Computer Vision and Pattern Recognition*. pp. 6469–6478 (2020) [3](#), [4](#)
36. Mahmood, N., Ghorbani, N., Troje, N.F., Pons-Moll, G., Black, M.J.: Amass: Archive of motion capture as surface shapes. In: *Proceedings of the IEEE/CVF international conference on computer vision*. pp. 5442–5451 (2019) [7](#)
37. McAuley, S., Hill, S., Hoffman, N., Gotanda, Y., Smits, B., Burley, B., Martinez, A.: Practical physically-based shading in film and game production. In: *ACM SIGGRAPH 2012 Courses*, pp. 1–7 (2012) [4](#), [6](#), [7](#)
38. Metzger, G., Richardson, E., Patashnik, O., Giryes, R., Cohen-Or, D.: Latent-nerf for shape-guided generation of 3d shapes and textures. In: *Proceedings of the IEEE/CVF Conference on Computer Vision and Pattern Recognition*. pp. 12663–12673 (2023) [2](#), [4](#), [10](#), [11](#), [12](#), [13](#)
39. Michel, O., Bar-On, R., Liu, R., Benaim, S., Hanocka, R.: Text2mesh: Text-driven neural stylization for meshes. In: *CVPR (2022)* [4](#)
40. Mohammad Khalid, N., Xie, T., Belilovsky, E., Popa, T.: Clip-mesh: Generating textured meshes from text using pretrained image-text models. In: *SIGGRAPH Asia 2022 conference papers*. pp. 1–8 (2022) [4](#)
41. Müller, T., Evans, A., Schied, C., Keller, A.: Instant neural graphics primitives with a multiresolution hash encoding. *ACM Transactions on Graphics (ToG)* **41**(4), 1–15 (2022) [4](#)
42. Ouyang, L., Wu, J., Jiang, X., Almeida, D., Wainwright, C., Mishkin, P., Zhang, C., Agarwal, S., Slama, K., Ray, A., et al.: Training language models to follow instructions with human feedback. *Advances in Neural Information Processing Systems* **35**, 27730–27744 (2022) [6](#)
43. Poole, B., Jain, A., Barron, J.T., Mildenhall, B.: Dreamfusion: Text-to-3d using 2d diffusion. *arXiv preprint arXiv:2209.14988* (2022) [4](#)
44. Radford, A., Kim, J.W., Hallacy, C., Ramesh, A., Goh, G., Agarwal, S., Sastry, G., Askell, A., Mishkin, P., Clark, J., et al.: Learning transferable visual models from natural language supervision. In: *International conference on machine learning*. pp. 8748–8763. PMLR (2021) [4](#), [9](#), [10](#), [12](#)
45. Renderpeople: Over 4,000 Scanned 3D People Models. <https://renderpeople.com/> (2023) [4](#)
46. Richardson, E., Metzger, G., Alaluf, Y., Giryes, R., Cohen-Or, D.: Texture: Text-guided texturing of 3d shapes. *arXiv preprint arXiv:2302.01721* (2023) [2](#), [4](#), [10](#), [11](#), [12](#), [13](#)
47. Rombach, R., Blattmann, A., Lorenz, D., Esser, P., Ommer, B.: High-resolution image synthesis with latent diffusion models. In: *Proceedings of the IEEE/CVF conference on computer vision and pattern recognition*. pp. 10684–10695 (2022) [2](#), [4](#), [6](#)
48. Ruiz, N., Li, Y., Jampani, V., Pritch, Y., Rubinstein, M., Aberman, K.: Dreambooth: Fine tuning text-to-image diffusion models for subject-driven generation. In: *Proceedings of the IEEE/CVF Conference on Computer Vision and Pattern Recognition*. pp. 22500–22510 (2023) [7](#)

49. Saito, S., Simon, T., Saragih, J., Joo, H.: Pifuhd: Multi-level pixel-aligned implicit function for high-resolution 3d human digitization. In: Proceedings of the IEEE/CVF Conference on Computer Vision and Pattern Recognition. pp. 84–93 (2020) [4](#)
50. Shen, K., Guo, C., Kaufmann, M., Zarate, J.J., Valentin, J., Song, J., Hilliges, O.: X-avatar: Expressive human avatars. In: Proceedings of the IEEE/CVF Conference on Computer Vision and Pattern Recognition. pp. 16911–16921 (2023) [4](#)
51. Su, Z., Yu, T., Wang, Y., Liu, Y.: Deepcloth: Neural garment representation for shape and style editing. *IEEE Transactions on Pattern Analysis and Machine Intelligence* **45**(2), 1581–1593 (2022) [3](#)
52. Svitov, D., Gudkov, D., Bashirov, R., Lempitsky, V.: Dinar: Diffusion inpainting of neural textures for one-shot human avatars. In: Proceedings of the IEEE/CVF International Conference on Computer Vision. pp. 7062–7072 (2023) [5](#)
53. Tang, J., Wang, T., Zhang, B., Zhang, T., Yi, R., Ma, L., Chen, D.: Make-it-3d: High-fidelity 3d creation from a single image with diffusion prior pp. 22819–22829 (October 2023) [4](#)
54. treedy’s: 3D body scanning technology. <https://www.treedys.com/> (2023) [4](#)
55. Twindom: Full Body 3D Scanners for 3D Printed Figurines, 3D Portraits and 3D Selfies. <https://web.twindom.com/> (2023) [4](#)
56. Varol, G., Romero, J., Martin, X., Mahmood, N., Black, M.J., Laptev, I., Schmid, C.: Learning from synthetic humans. In: Proceedings of the IEEE conference on computer vision and pattern recognition. pp. 109–117 (2017) [4](#)
57. Wang, J., Zhong, Y., Li, Y., Zhang, C., Wei, Y.: Re-identification supervised texture generation. In: Proceedings of the IEEE/CVF Conference on Computer Vision and Pattern Recognition. pp. 11846–11856 (2019) [10](#)
58. Wang, P., Liu, L., Liu, Y., Theobalt, C., Komura, T., Wang, W.: Neus: Learning neural implicit surfaces by volume rendering for multi-view reconstruction. arXiv preprint arXiv:2106.10689 (2021) [4](#)
59. Wang, Z., Bovik, A.C., Sheikh, H.R., Simoncelli, E.P.: Image quality assessment: from error visibility to structural similarity. *IEEE transactions on image processing* **13**(4), 600–612 (2004) [10](#)
60. Xiu, Y., Yang, J., Cao, X., Tzionas, D., Black, M.J.: Econ: Explicit clothed humans optimized via normal integration. In: Proceedings of the IEEE/CVF Conference on Computer Vision and Pattern Recognition. pp. 512–523 (2023) [4](#)
61. Xu, C., Zhu, J., Zhang, J., Han, Y., Chu, W., Tai, Y., Wang, C., Xie, Z., Liu, Y.: High-fidelity generalized emotional talking face generation with multi-modal emotion space learning. In: CVPR (2023) [3](#)
62. Xu, X., Chen, H., Moreno-Noguer, F., Jeni, L.A., De la Torre, F.: 3d human pose, shape and texture from low-resolution images and videos. *IEEE transactions on pattern analysis and machine intelligence* **44**(9), 4490–4504 (2021) [10](#)
63. Xu, X., Loy, C.C.: 3d human texture estimation from a single image with transformers. In: Proceedings of the IEEE/CVF international conference on computer vision. pp. 13849–13858 (2021) [4](#), [10](#), [11](#), [12](#), [13](#)
64. Yang, Z., Zeng, A., Yuan, C., Li, Y.: Effective whole-body pose estimation with two-stages distillation. In: Proceedings of the IEEE/CVF International Conference on Computer Vision. pp. 4210–4220 (2023) [6](#)
65. Yang, Z., Cai, Z., Mei, H., Liu, S., Chen, Z., Xiao, W., Wei, Y., Qing, Z., Wei, C., Dai, B., Wu, W., Qian, C., Lin, D., Liu, Z., Yang, L.: Synbody: Synthetic dataset with layered human models for 3d human perception and modeling (2023) [3](#)

66. Youwang, K., Ji-Yeon, K., Oh, T.H.: Clip-actor: Text-driven recommendation and stylization for animating human meshes. In: European Conference on Computer Vision. pp. 173–191. Springer (2022) [2](#)
67. Yu, F., Seff, A., Zhang, Y., Song, S., Funkhouser, T., Xiao, J.: Lsun: Construction of a large-scale image dataset using deep learning with humans in the loop. arXiv preprint arXiv:1506.03365 (2015) [7](#)
68. Yu, T., Zheng, Z., Guo, K., Liu, P., Dai, Q., Liu, Y.: Function4d: Real-time human volumetric capture from very sparse consumer rgbd sensors. In: Proceedings of the IEEE/CVF conference on computer vision and pattern recognition. pp. 5746–5756 (2021) [3](#), [4](#)
69. Zeng, Y., Lu, Y., Ji, X., Yao, Y., Zhu, H., Cao, X.: Avatarbooth: High-quality and customizable 3d human avatar generation. arXiv preprint arXiv:2306.09864 (2023) [2](#), [4](#)
70. Zhang, C., Pujades, S., Black, M.J., Pons-Moll, G.: Detailed, accurate, human shape estimation from clothed 3d scan sequences. In: Proceedings of the IEEE Conference on Computer Vision and Pattern Recognition. pp. 4191–4200 (2017) [3](#), [4](#)
71. Zhang, J., Zeng, X., Wang, M., Pan, Y., Liu, L., Liu, Y., Ding, Y., Fan, C.: Freenet: Multi-identity face reenactment. In: CVPR (2020) [3](#)
72. Zhang, L., Rao, A., Agrawala, M.: Adding conditional control to text-to-image diffusion models. In: Proceedings of the IEEE/CVF International Conference on Computer Vision. pp. 3836–3847 (2023) [6](#)
73. Zhang, R., Isola, P., Efros, A.A., Shechtman, E., Wang, O.: The unreasonable effectiveness of deep features as a perceptual metric. In: Proceedings of the IEEE conference on computer vision and pattern recognition. pp. 586–595 (2018) [10](#)
74. Zhao, F., Liao, S., Zhang, K., Shao, L.: Human parsing based texture transfer from single image to 3d human via cross-view consistency. Advances in Neural Information Processing Systems **33**, 14326–14337 (2020) [4](#), [5](#), [10](#)
75. Zheng, K., He, X., Wang, X.E.: Minigt-5: Interleaved vision-and-language generation via generative vokens. arXiv preprint arXiv:2310.02239 (2023) [9](#)
76. Zheng, L., Shen, L., Tian, L., Wang, S., Wang, J., Tian, Q.: Scalable person re-identification: A benchmark. In: Proceedings of the IEEE international conference on computer vision. pp. 1116–1124 (2015) [4](#), [11](#), [12](#)
77. Zheng, Z., Yu, T., Liu, Y., Dai, Q.: Pamir: Parametric model-conditioned implicit representation for image-based human reconstruction. IEEE transactions on pattern analysis and machine intelligence **44**(6), 3170–3184 (2021) [4](#)
78. Zheng, Z., Yu, T., Wei, Y., Dai, Q., Liu, Y.: Deephuman: 3d human reconstruction from a single image. In: Proceedings of the IEEE/CVF International Conference on Computer Vision. pp. 7739–7749 (2019) [3](#), [4](#)

Appendix

In this appendix, Appendix A provides more information regarding the ATLAS dataset construction. Appendix B presents more analysis of TexDreamer training. Appendix C show more qualitative results of TexDreamer, including both text-to-UV and image-to-UV. We also present more human textures included in our ATLAS dataset.

A More Details of ATLAS Construction

Text Augmentation. To acquire multi-view images for fictional characters, we use text augmentation to promote the consistency of generated character identities. Tab. 6 provides details about view-related and other description prompts. The positive prompt T_{pos} is used to condition the main generation direction. We describe T_{pos} with character identity T_{id} , generate poses T_{pose} and other descriptions T_{other} .

ChatGPT Prompt Structure. We divide avatar descriptions into four categories: detailed description, fictional character, celebrity, and general description. For each category, we design distinct generation templates. For each category in Fig. 9, “[]” content is included with every prompt, “()” indicates the content appears randomly.

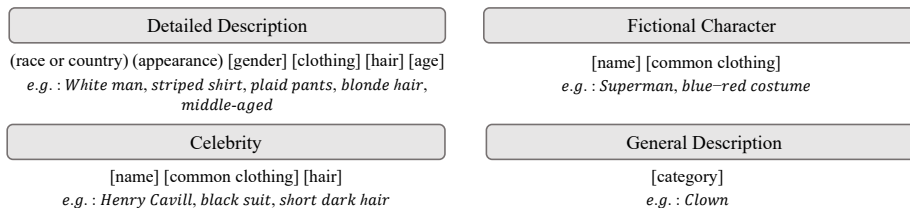
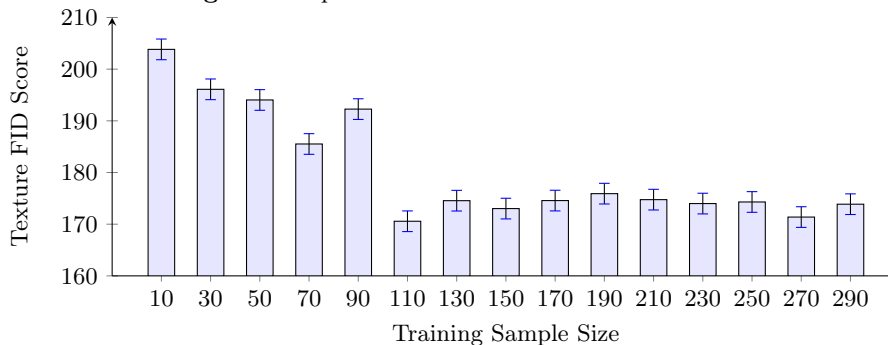
Materials. We provide more material settings for rendering textured humans. To achieve authentic human-like material, we set “dielectric specular reflection” to 0.1, and increase the “Roughness” to 0.6. Moreover, “Sheen Tint” is 0.5, “Clearcoat Roughness” is 0.03, and “Index of refraction for transmission” (IOR) is 1.45. The “Alpha” channel remains to be 1.

B More Analysis of TexDreamer

Training Sample Size. Different training sample sizes can have different influences on model generation ability. We use the FID score to evaluate different training sizes. FID score measures the similarity between the distribution of generated images and the distribution of real images. Lower FID values mean

Table 6: Overview of prompts we used for ATLAS sample texture image generation.

		T_{pos}	T_{neg}
view	front	front side, from front, the front of T_{id}	backside
	back	backside, from back, the backside of T_{id}	front, face, head
	left	left side, from left	front, back
	right	right side, from right	front, back
other	black background, diffuse rendering, daylight	overexposed, nude, layman work, worst quality, teeth, smile, open mouth, eyes closed	

**Fig. 9:** Prompt structure for ATLAS construction.**Fig. 10:** Correlation between Training Sample Size and Texture FID Score.

better image quality and diversity. Toward human texture generation from text, T2UV, we experiment with sample size spans from 10 to 300 with an interval of 20, see results in Fig. 10. We find that the FID score between each test set and its train set tends to gradually start to become consistent over 100 training samples. This indicates that the model has reached a point of saturation with the given training data. In other words, the model learned the UV structure using around 100 textures, adding more training samples will not continue to contribute to improving model’s ability to generate new, diverse, and high-quality textures.

C More Qualitative Results

We show more qualitative results of TexDreamer and ATLAS. For generating textures from text, we show more results including both realistic humans and fictional characters in Fig. 11, Fig. 12, and Fig. 13. Meshes are generated with text-to-avatar method TADA, and we animate the fictional characters with Mixamo. Fig. 14 also show more results with textures generated from images. Moreover, we display more human textures included in our ATLAS dataset, see Fig. 15, Fig. 16 and Fig. 17.



Russian man, white crew neck t-shirt, black joggers, brown hair



Latino man, leather jacket, cargo shorts, black hair, teenager



North Korean man, denim T-shirt, short sleeves, capri jeans, black hair, young adult



Brazilian man, pink polo shirt, white dress pants, dark brown hair



charming man, green varsity jacket, black harem pants, light brown hair, young adult



Middle eastern man, blue denim jacket, blue jeans, black hair



Mexican man, windbreaker, white gym shorts, black hair, teenager



attractive man, burgundy turtleneck, white pinstripe pants, light brown hair

Fig. 11: Realistic human textures generated from text with TexDreamer, each rendered with the same mesh.



African man, orange long sleeve shirt, denim shorts, light brown hair



Latino man, grey streetwear t-shirt, black jeans, black hair, urban



Middle Eastern man, tweed blazer, light khaki dress pants, gray hair, elderly



handsome white man, white jacket, black pants, blonde hair



Latino man, formal black suit, dress trousers, brown hair, distinguished



Arabian man, silver tuxedo, dark grey dress pants, gray hair, elderly, monocle



Hispanic man, rugged flannel shirt, denim jeans, black hair



African man, muscle tee, drawstring light khaki shorts, light brown hair

Fig. 12: Realistic human textures generated from text with TexDreamer, each rendered with the same mesh.



The Hulk



Pretty woman, stunning gold blouse, brown leggings



Spiderman



Geralt of Rivia in The Witcher



The Flash



Black Widow



Link in The Legend of Zelda



Iron man

Fig. 13: Fictional character textures generated from text with TexDreamer.

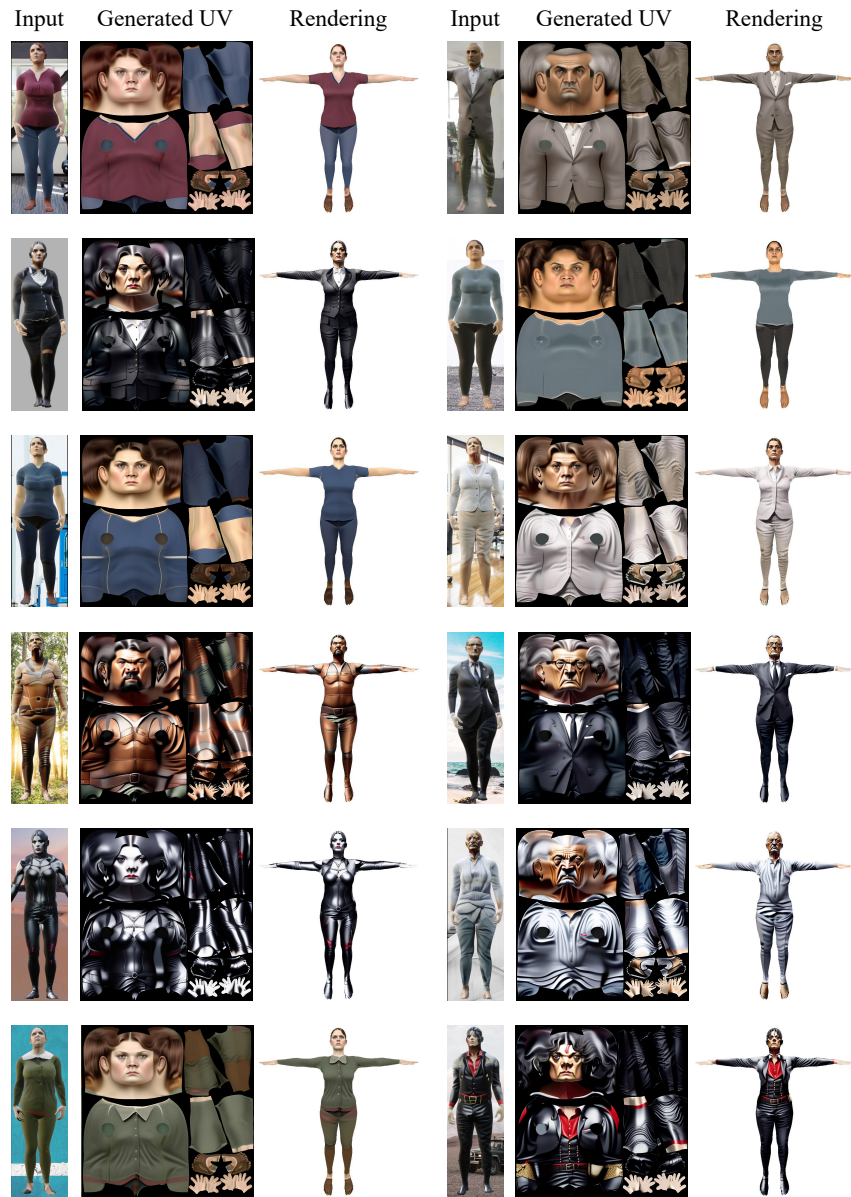


Fig. 14: Texture generated from images with TexDreamer.



Fig. 15: Human textures in our ALTAS dataset, example set 1.



Fig. 16: Human textures in our ALTAS dataset, example set 2.



Fig. 17: Human textures in our ALTAS dataset, example set 3.